

Automatic Passenger Counting in the High Occupancy Vehicle (HOV) Lanes

I. Pavlidis

P. Symosek

B. Fritz

Honeywell Technology Center
3660 Technology Drive
MN65-2500
Minneapolis, MN 55418
Tel. (612) 951-7338
Fax (612) 951-7438
(pavlidis, symosek, fritz)@htc.honeywell.com

R. Sfarzo

N. P. Papanikolopoulos

University of Minnesota
Department of Computer Science and Engineering
200 Union Street S.E.
Minneapolis, MN 55455
Tel. (612) 625-0163
Fax (612) 625-0572
(sfarzo, npapas)@cs.umn.edu

Abstract

The gathering of usage statistics in the High Occupancy Vehicle (HOV) lane is mandated by the Federal Highway Administration. These statistics are crucial for construction planning. Currently, the gathering of data is performed manually. This is obviously laborious, inefficient, and prone to error. Under a Minnesota Department of Transportation (Mn/DOT) contract we undertook a study to determine if the automatic counting of passengers is feasible. In the present paper we report our findings regarding the appropriate sensor phenomenology and arrangement for the task and our plans for the future.

Introduction

The Honeywell Technology Center (HTC) in cooperation with the University of Minnesota (U of MN) carries out a feasibility study regarding the automatic counting of car passengers in the HOV lane of freeways. The study is funded by Mn/DOT.

There are compelling reasons for the existence of an automatic passenger counting system in the HOV lane. It will facilitate the gathering of statistical data for road construction planning. It will enable state authorities to charge a nominal fee to single passenger vehicles. It will also help the State Patrol to perform its monitoring task more effectively.

The passenger counting system needs to be reliable. In a sensing system, reliability is rarely achieved if the signal is corrupted with noise. The first concern in the present effort is to produce a signal with as distinct a signature for the car passenger as possible. Our study so far has confirmed that this goal can be achieved only through careful selection and arrangement of the sensing elements.

The rest of this paper is organized as follows: First, we comment upon some other relevant work. Second, we describe our findings during the first half period of the study. This work falls under the first task of the HOV project, *Data Collection and Fusion*, which was completed by October 1998. Third, we outline the remaining work to be done under the task of Algorithm Development. Actually, work in the Algorithm Development task is under way and is briefly mentioned in this document. Finally, we acknowledge the contribution of certain organizations and individuals.

Relevant Work

Our effort during the first half of the project's period was primarily concentrated in the task of *Data Collection and Fusion*. The objectives in this task were:

1. Select the appropriate sensors and accessories.
2. Design an appropriate sensor arrangement.

We have completed this task and fulfilled all its objectives. This was the most important task of the project since its successful conclusion was critical to the success of the entire project. The reason for this was simple: If we managed to acquire a clear imaging signal through the sensors, then even moderately powerful pattern recognition algorithms would accomplish the passenger detection task. If, however, the imaging signal were noisy, then even the most powerful pattern recognition algorithms would break.

Upon embarking on our effort in late April 1998 we were aware of one other similar study worldwide led by the Georgia Tech Research Institute (GTRI). The effort involved the use of a near-infrared camera (0.55 - 0.90 μm) and a near-infrared illumination source in the same range. One reason for using near-infrared sensing was the ability to use non-distracting illumination during the night. Illumination during nighttime certainly enhances the quality of the image. We believe, however, that the choice of the band is not appropriate because of its close proximity to the visible spectrum. Psychophysical experiments have shown that the human eye has some sensitivity to this band of near-infrared, however small. This may be enough to cause potentially accidents under certain conditions. Another reason for this approach, according to the GTRI investigators, was to bypass the problems caused by solar illumination during daytime, such as glare. Nevertheless, particularly in the range (0.55 - 0.9 μm) solar illumination is still substantial and the associated glare can be reduced only through the use of polarizing filters.

In more general terms, Intelligent Transportation Systems (ITS) projects that involve imaging usually adopt the use of visible spectrum cameras. The strong point of the visible spectrum approach is that the relevant imaging sensors are the most advanced and at the same time the cheapest across the Electro-Magnetic (EM) spectrum. Visible spectrum cameras have a particular advantage in terms of speed, which is an important consideration in the HOV lane where vehicles are moving at rates of speed of 65 mph. They can also have very high resolution, which accounts for very clear images under certain conditions. Unfortunately, there are also a lot of serious problems with the visible spectrum approach. To mention a few: Some vehicles have heavily tinted window glass to reduce glare from solar illumination; this glass is almost opaque to visible spectrum cameras. Also, visible spectrum cameras don't have operational capability during nighttime.

Data Collection and Fusion

Methodology

One factor that is distinctly absent in the aforementioned research efforts, and unfortunately, in many other computer vision projects is a vigorous sensor phenomenology study. Most researchers without a second thought adopt the visible spectrum as the spectrum of choice, or, in rare cases, some other EM spectrum based primarily on intuition. The result is that they usually end up with a non-discriminating signal that makes the problem appear harder than it actually is. Then, they try to address the difficulty by devising powerful computer vision algorithms but often to no avail. The loss of information because of poor sensor choice and arrangement is usually irrevocable.

Our first consideration was to look into what nature had to offer across the EM spectrum (see Figure 1). The lower portion of the EM spectrum consists of the gamma rays, the x-rays, and the ultra-violet range. They are all considered harmful and they are used in a controlled manner in medical applications only. Then, the visible spectrum, is the range we are mostly acquainted with since it is used by the human eye and the vast majority of cameras. Visible spectrum cameras use mature technology and they feature the best quality to price ratio. They achieve very high resolution and speed, and with the recent introduction of digital technology negligible systemic noise levels. Unfortunately, their systemic noise levels increase during poor environmental conditions like bad weather, nighttime, direct sunlight. Some of these weaknesses are incurable. Some others, like nighttime, can be overcome by using artificial lighting. Nevertheless, this is not an option in the case of transportation applications. The artificial light should match the spectrum of the camera (visible range) and consequently it will distract the drivers with perhaps fatal results. One other characteristic, that is very important in computer vision applications, is also absent in this range. The image understanding task becomes feasible or easier when the object of interest, the human face in our case, appears to have consistent qualities under a variety of conditions. In visible spectrum cameras, the passenger faces appear darker or lighter depending on the physical characteristics of the passenger, the incident angle of illumination, and the illumination intensity.

At the far end of the EM spectrum there are the microwave and radio regions. This area was just started to be exploited for imaging purposes. Sensors operate in active or in passive mode. The major advantage is that the long wavelengths in these regions can penetrate clouds, fog, and rain producing weather-independent imaging results. The technology is very new, and thus prohibitively expensive. Also the sensors are bulky, and feature very low resolution. Their application is currently constrained in the military and the remote-sensing domain [1].

Between the low and the far end of the EM spectrum there is a middle region, which is known as the infrared range (0.7 - 100 μm). Within the infrared range, two bands of particular interest are the Reflected Infrared (0.7 - 3.0 μm) and the thermal infrared (3.0 - 5.0 μm , 8.0 - 14. μm) bands. The reflected infrared band on one hand is associated with reflected solar radiation that contains no information about the thermal properties of materials. This radiation is for the most part invisible to the human eye. The thermal infrared band on the other hand is associated with the thermal properties of materials.

Mid-Infrared Approach

Upon embarking in our study we concentrated on the thermal infrared region for the following reasons:

1. The human body maintains a relatively constant temperature (about 36.6⁰ Celsius) irrespectively of physical characteristics or illumination conditions. This would translate into a consistent light color pattern for the faces of the car passengers in infrared imaging. This consistency is lacking in the visible spectrum and would greatly facilitate the image understanding task. Incidentally, the thermal property can serve as a differentiator between humans and dummies.
2. A thermal infrared sensor is operational day and night without any need for an external illumination source.

Our only concern was the attenuation introduced by the presence of the vehicle glass. Glass disrupts severely the transmission of infrared illumination beyond 2.8 μm . This is the range where thermal energy is just beginning to appear. If we were to capture anything at all we needed an extremely sensitive mid-infrared camera in the range 2.0 - 3.0 μm . The Mitsubishi Thermal Imager IR-700 proved to be the appropriate sensor for the task. An additional consideration was the composition of the glass in vehicle windows. Vehicle windows are not made from common glass for a variety of reasons (safety, energy efficiency, and visibility). Notably, the composition of the front windshield differs substantially from the composition of the side windows. Spectral measurements for a typical vehicle windshield (see Figure 2) compared with spectral measurements for a typical side window glass (see Figure 3), revealed that it would be beneficial to place the infrared camera by the side of the road. Initial experiments with the Mitsubishi camera confirmed these theoretical predictions. We could not see anything inside the vehicles when we were shooting in frontal view. In contrast, we were getting very clear images when we were shooting from the side.

These initial experiments were performed in a parking lot with the test vehicle either stationary or moving at low speed (up to 20 mph). We performed one such experiment in winter, even before the official start of the program and one in spring. The side view images were very clear (see Figure 4) except in one case. That was in wintertime when the vehicle's defogger was on for more than half an hour. Then, the thermal signature of the air in the interior of the vehicle was becoming stronger than the thermal signature of the passengers. The result was a cluttered imaging signal.

In a third experiment, in spring, we took our testing to an actual highway site (I394). This time we were shooting from the side of the freeway at vehicles moving at speeds of 65 mph. As always, we were using the infrared camera side by side with our digital visible spectrum Sony DSR 200 camera. The results showed that the mid-infrared camera was not capable of capturing clear images of such fast moving targets (see Figure 5). The Mitsubishi IR-700 operates at a frequency of 30 Hz. In comparison, the visible spectrum camera was operating at 1000 Hz to achieve clear images of such fast moving targets. Unfortunately, mid-infrared technology cannot afford such a high frequency rate at the present time. The situation would be better if the infrared camera were able to penetrate the front windshield, because in frontal view the vehicle remains in the camera's field of view for more time. Consequently, this would impose less severe speed capture demands. But, placing the mid-infrared camera in frontal view is not an option since it cannot penetrate the front windshield. That left us in a deadlock and we turned our attention to the reflected infrared band and particularly the range 1.0 - 2.0 μm .

Near-Infrared Approach

The first concern was to find a state of the art camera sensitive in the reflective near-infrared band that can be consigned to us for experimentation, much the same way as the Mitsubishi IR-700 did. Sensors Unlimited Inc. agreed to consign us their SU-320 near-infrared camera that fulfilled our specification. We performed two preliminary rounds of experiments in HTC's parking lot with the SU-320. The first round took place in spring and the second in summer. Based on this experience and subsequent theoretical investigation, we determined that the SU-320 camera could live up to the challenges of the HOV requirements if certain steps are taken. Specifically:

1. We found theoretically and experimentally a unique differentiator for the human face in the range 1.4 - 1.7 μm that substitutes the corresponding thermal differentiator of the mid-infrared range. Above 1.4 μm human skin appears consistently dark irrespectively of the persons physical characteristics (Figure 6 - Figure 9) [2]. The phenomenon is exemplified in Figure 10 and Figure 11. In Figure 11, a Caucasian male is pictured next to a dummy head when the near-infrared camera is equipped with a band pass filter in the range 1.1 - 1.4 μm . They both appear in a relatively lighter color than the background close to the way they would appear in the visible spectrum. In Figure 10 the same Caucasian male and dummy head show different when the camera is equipped with a band pass filter in the range 1.4 - 1.7 μm . In fact, the face of the white Caucasian male appears dark (darker than the background). The face of any other human would exhibit this behavior irrespectively of its physical characteristics. In contrast, the dummy head appears as a light colored object (lighter than the background), easily distinguishable from the human head. This sort of response is shared by many other inanimate objects that can be found inside a vehicle like for example upholstery, dashboard, fabrics (see Figure 12). The low reflectivity of human flesh for the 1.4 - 1.7 μm can be explained if we notice the spectral response of the water in the same

region. Beyond $1.4 \mu\text{m}$ the water absorbs substantially infrared radiation and appears in the image as a dark body (see Figure 13). Since the composition of the human body consists of 70% water naturally, its spectral response is very similar to that of the water. Hence, the camera should be equipped with a $1.4 - x \mu\text{m}$ (where $x > 1.4 \mu\text{m}$) band pass filter to capture this unique passenger differentiator.

2. The solar illumination in the range $1.4 - x \mu\text{m}$ (where $x > 1.4 \mu\text{m}$) creates a lot of glare effects that lessen the quality of the imaging signal. A polarizing filter is needed during daytime to improve the quality of the image.
3. The operating range $1.4 - 1.7 \mu\text{m}$ (where $x > 1.4 \mu\text{m}$) is quite apart from the visible band and we can quite safely employ during nighttime a matching near-infrared illumination source to improve the quality of the image. The light will not only be invisible to the drivers but also completely harmless to their eyes since its wavelength is above the safe threshold of $1.4 \mu\text{m}$.
4. Since we operate at a lower band than the mid-infrared band, glass penetration is not a problem and we can easily see through the frontal windshield. This makes the speed requirements for the camera less stringent. In the actual highway site, where shooting will be performed from a distance, probably a zoom lens will be required. In general, a complete optical design seemed to be in order that would verify mathematically the feasibility of the approach.

Radiometric Calculation

We undertook a complete optical design of the near-infrared experimental setup that proved theoretically the feasibility of the approach. Figure 14 shows the layout of the proposed near-infrared system during daytime. We assume that a vehicle is moving down a highway with velocity v and is observed in frontal view with the near-infrared SU-320 camera at a distance d and from a height h . We also assume that the SU-320 camera is equipped with the following accessories:

1. A telephoto lens.
2. A band-pass filters in the range $1.4 - x \mu\text{m}$ (where $x > 1.4 \mu\text{m}$).
3. A polarizing filter to reduce the glare effect from the sun illumination during daytime.

During daytime the system uses the illumination of the sun. The objective is to determine if there is any appropriate geometric arrangement for the SU-320 camera so that the signal to noise (S/N) ratio and the camera speed are kept at acceptable levels even under adverse conditions. An acceptable (S/N) ratio is considered anything above 35. The speed quality is considered acceptable when the image smearing does not exceed the width of one pixel.

The first step in a radiometric computation is to determine the amount of radiation that falls upon the objects of interest [3] - in our case the vehicle passengers. As we stated, we consider a spectral band, above the $1.4 \mu\text{m}$ threshold point. Because of constraints due to the quantum efficiency of the SU-320 camera we limit the spectral band in the range $1.4 - 1.7 \mu\text{m}$. The spectral radiance of the sun (our illumination source) on a clear day at sea level is

approximately $R_{\text{sunny}} = 0.008 \text{ Watts/cm}^2$ in the 1.4 - 1.7 μm wave-band. In our computation, however, we consider the worst case scenario of an overcast day. For an overcast day the radiance value is reduced by 10^{-3} giving radiance at the vehicle of approximately

$$\begin{aligned} R_{\text{overcast}} &= 10^{-3} * R_{\text{sunny}} \\ &= 10^{-3} * 0.008 \\ &= 8 \mu\text{Watts/cm}^2. \end{aligned}$$

The transmission of the windshield of the vehicle is approximately 0.4 resulting in an irradiance on the vehicle occupants of

$$\begin{aligned} I_{\text{passenger}} &= 0.4 * R_{\text{overcast}} \\ &= 0.4 * 8 \\ &= 3.2 \mu\text{Watts/cm}^2. \end{aligned}$$

The second step in a radiometric computation is to determine how much of the incident radiation on the objects of interest is reflected back to the sensor (the SU-320 near-infrared camera in our case). The radiance into a hemisphere assuming a reradiate of 0.4 would be

$$\begin{aligned} R_{\text{passenger}} &= 0.4 * I_{\text{passenger}} / \pi \\ &= 0.4 * 3.2 / \pi \\ &= 0.4 \mu\text{Watts} / \text{cm}^2 - \text{ster}. \end{aligned}$$

This represents the reflected portion of the passenger irradiation. The passenger's body absorbs the rest. The reflected radiation has to pass through the windshield and the camera lens to reach the near-infrared sensor array. Assuming a f/2 camera lens (14.32⁰ cone angle) with a transmission of 0.8 and windshield transmission of 0.4 the irradiance at the sensor array of the SU-320 camera will be

$$\begin{aligned} I_{\text{camera}} &= 0.4 * 0.8 * 0.4 * 0.6 * \pi * R_{\text{passenger}} * \sin^2(14.32^0) \\ &= 0.4 * 0.8 * 0.4 * 0.6 * \pi * 0.4 * \sin^2(14.32^0) \\ &= 0.006 \mu\text{Watts/cm}^2. \end{aligned}$$

The SU-320 camera has square pixels with a side of $37.5 * 10^{-4} \text{ cm}$ or an area

$$\begin{aligned} A &= 37.5 * 10^{-4} * 37.5 * 10^{-4} \\ &= 1.40 * 10^{-5} \text{ cm}^2. \end{aligned}$$

Consequently, the radiant power on the camera pixel will be

$$\begin{aligned} P_{\text{pixel}} &= A * I_{\text{camera}} \\ &= 1.4 * 10^{-5} * 0.006 \\ &= 0.084 * 10^{-12} \text{ Watts}. \end{aligned}$$

The camera's detectivity D^* is $D^* = 10^{12} \text{ cm } \sqrt{\text{Hz}} / \text{Watts}$. The Noise Equivalent Power NEP is related to detectivity D^* , pixel area A , and electronic bandwidth Δf by the following equation:

$$\text{NEP} = (A / \Delta f)^{1/2} / D^*.$$

The bandwidth Δf is determined by the exposure time of the camera. The exposure time depends on the vehicle velocity, the camera range, and the camera field of view such that the images smear less than 1 pixel. Assuming a vehicle traveling at a speed of 65 mph, a distance d of 40 m apart from the camera, and a field of view of 1.6 m, the 320×240 pixel array of SU-320 gives a maximum exposure time of 1 msec or a bandwidth of $\Delta f = 1 \text{ KHz}$. Substituting the values for A , Δf , and D^* in the formula of NEP we get

$$\text{NEP} = 1.18 * 10^{-13} \text{ Watts}.$$

Therefore, the signal to noise ratio S/N will be

$$S/N = P_{\text{pixel}} / \text{NEP} = 0.7.$$

In conclusion, assuming a worst case scenario (overcast day, dirty windshield, dark passenger skin) we determined that the SU-320 camera, equipped with a $f/2$ lens, a $1.4\text{-}1.7 \mu\text{m}$ filter, and a polarizer, if it is positioned at a distance of $d = 40 \text{ m}$ from the incoming car and at a height of $h = 7 \text{ m}$ at the specified distance, will achieve:

1. An acceptable smear of less than one pixel because the required exposure time of 1 msec is within the camera's speed capabilities.
2. A poor signal to noise ratio $S/N = 0.7$. To boost the S/N ratio to a higher value in overcast days we need to employ an illumination source. This illumination source will also be helpful during nighttime. If we operated in the visible spectrum the use of illuminator in the HOV lane would be prohibitive. Fortunately, in our case the spectral signature of the illuminator for this range can be safely employed in the HOV lane.

We have performed the final experiments in the near-infrared band according to the theoretical specifications. The results of these experiments will be reported to another forum.

Future Work

Ongoing and future work that falls under the task of Algorithm Development is concentrated on two areas:

1. Improvement of the discriminating characteristics of the passengers in the imaging signal.
2. Design and development of the neural network that will perform the automatic passenger detection.

Work on the neural network is under way. Our passenger detection approach is based upon image segmentation and supervised learning. The incoming image is segmented first into

homogeneous sub-parts. The algorithm locates within these segments first the car, then the windshield, finally, the segments that are within the perimeter of the windshield. The major challenge at this point is to find which of these particular segments belong to the passengers (as opposed to, say, vehicle seats). The problem is more complicated than it appears because segmentation is rarely perfect and passengers usually consist of multiple loosely coupled segments. We apply supervised learning to discriminate passenger clusters of segments from non-passenger clusters of segments.

In the *forward learning* phase we incrementally present to the neural network a training set of segmented images that were collected and ground-truthed during the data collection phase. These images contain some segments that are passengers (*positive examples*) and some that are not (*negative examples*). The network classifies each segment or cluster of segments and outputs a number that represents its confidence that this is a passenger.

At the next *backward learning* phase we tell the network whether it was correct or not, and the network learns by modifying its structure slightly. We measure the success rate using a test set of similar images. The entire process of providing positive and negative examples, querying the network, improving performance continues until the network converges.

At a more detailed level, the inputs to the network represent *features* that describe the image. Some examples of these features include: shape, length, elongation, roughness, mean intensity values. It is important that we represent our knowledge of the input image in a manner that is invariant to transformations such as scale. For example, consider that we use the length feature: the focal length of the camera may vary causing the length of a person's head to vary as well. Therefore, a more suitable solution would be to use the normalized feature calculated as the relative length of an object inside the window to the entire window length.

We are currently developing a *multi-layer-feed-forward neural network* using *back-propagation error correction* [4]. The number of inputs varies as we experiment with the input vector of feature values. There is one output node. There is also a single hidden layer between the input layer and output node. The *sigmoid function* calculates each node's activation. The learning rate for all nodes is both static and identical. Weights are initialized randomly.

We did not choose to apply a neural network to the HOV problem by chance. Neural networks offer a lot of design flexibility. They may vary according to connectivity, input and output representations, the manner of error correction, and the rate at which they learn. These variable parameters must be manually fine-tuned with careful experimentation. This process may be time consuming but worthwhile. Neural networks are capable of classifying complex patterns such as the ones we face in this study. In addition, the run-time performance of a well-tuned neural network is very efficient.

Acknowledgements

We would like to extend our deep appreciation to Kevin Schwartz, the Mn/DOT HOVL program manager for his generous help and support. Many thanks to Ben Worel and Jack Herndon for accommodating our needs in the Mn/ROAD facility. We would also like to thank Joe Keller for his help during the road tests. Finally, we would like to thank Scott Nelson for a valuable discussion regarding some technical issues in this project. This work was supported by Mn/DOT under contract #F10041. The views and conclusions contained in this document are those of the authors and should not be interpreted as representing the official policies, either expressed or implied, of the funding agency.

Endnotes

1. F.E. Sabins, "Remote Sensing: Principles and Interpretation", W.H. Freeman and Company, New York, third edition, 1997.
2. J.A. Jacquesz, J. Huss, W. McKeenan, J.M. Dimitroff, and H.F. Kuppenheim, "The spectral reflectance of human skin in the region 0.7 - 2.6 μm ", Technical Report 189, Army Medical Research Laboratory, Fort Knox, April 1995.
3. B. K. P. Horn, Robot Vision, pages 202 - 277, The MIT Press, Cambridge, Massachusetts, 1986.
4. J. A. Freeamn, Simulating Neural Networks with Mathematica, Addison Wesley, 1994.

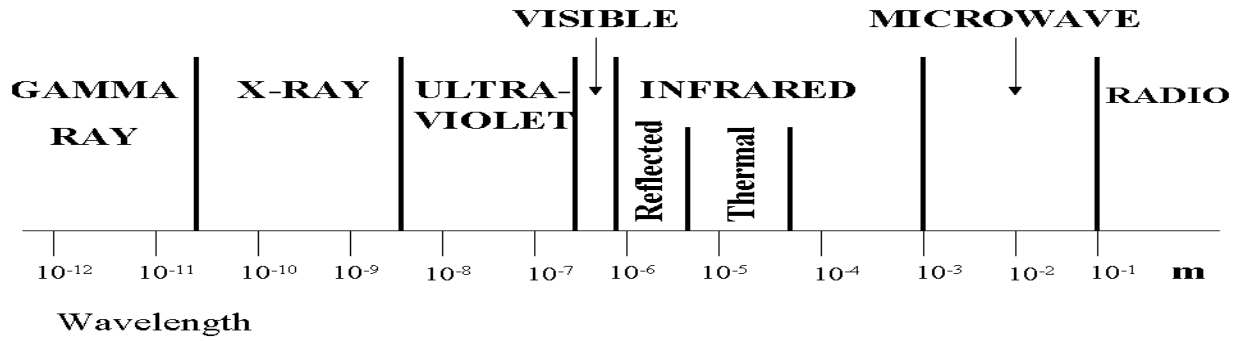


Figure 1: Electro-Magnetic (EM) spectrum.

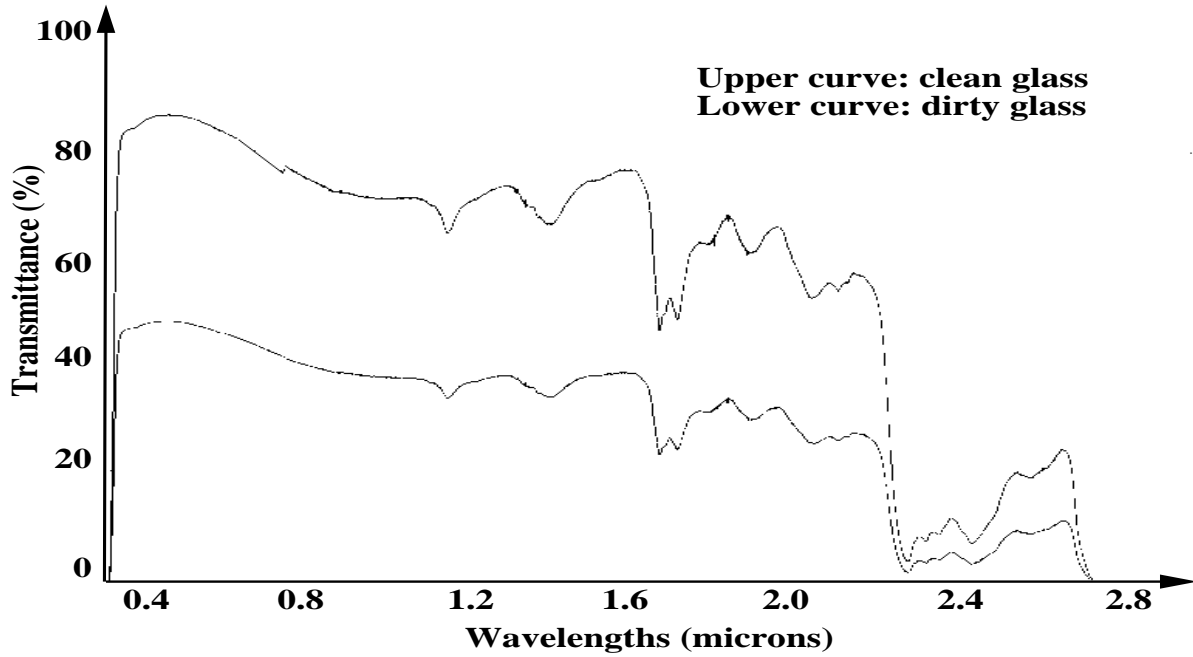


Figure 2: Transmittance of a typical windshield from 0.3 - 3.0 μm . Upper curve corresponds to a clean windshield. Lower curve corresponds to the same windshield when it gets dirty.

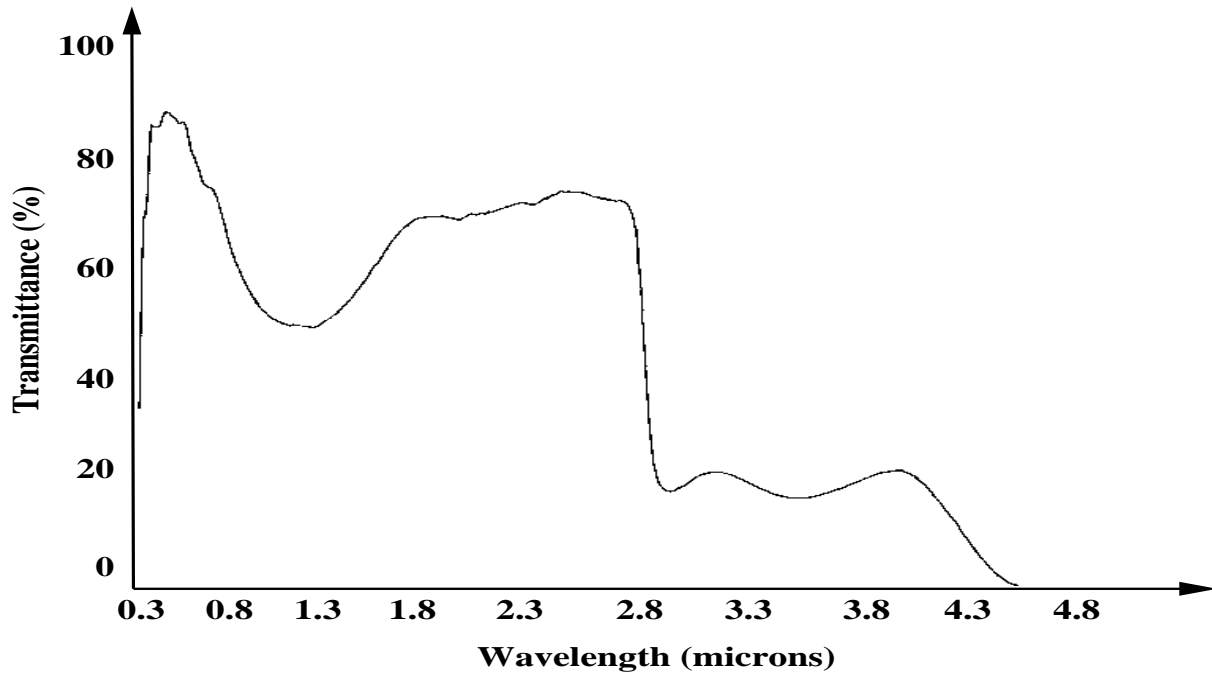


Figure 3: Transmittance of a lightly tinted side window from 0.3 - 3.0 μm . It is evident the graceful drop in transmittance even after the critical threshold of 2.8 μm . This spectral behavior allows for penetration of some thermal radiation. Compare this with the windshield transmittance in **Figure 2**.



Figure 4: Side snapshot of a low speed car with a mid-infrared camera.

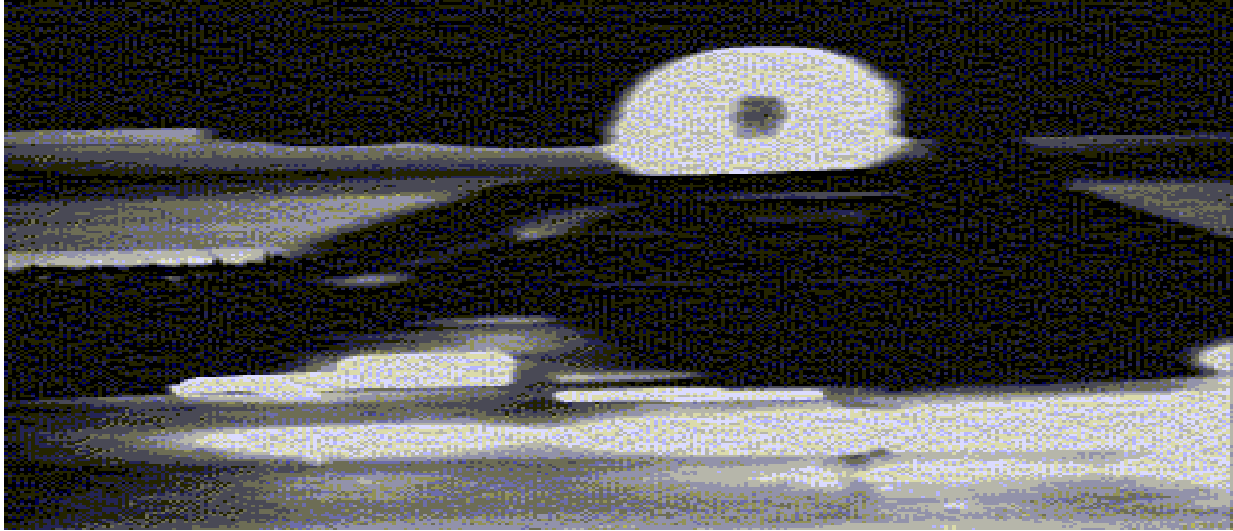


Figure 5: Side snapshot of a fast moving car (65 mph) with a mid-infrared camera. The image appears heavily blurred since the speed of the camera cannot keep up with the speed of the target.

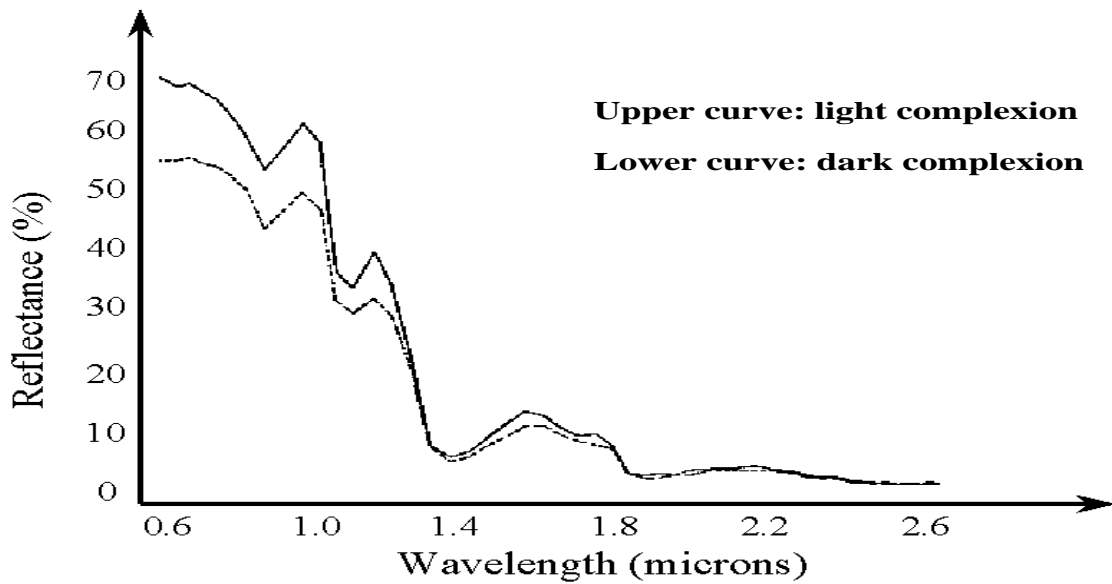


Figure 6: Skin reflectance of Caucasian males. Upper curve corresponds to light complexion while lower curve to dark complexion.

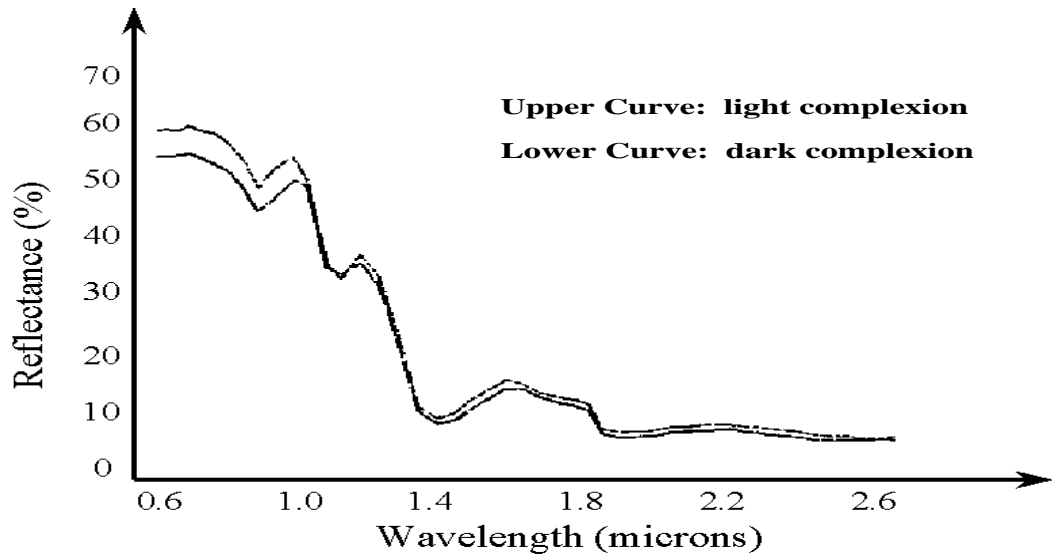


Figure 7: Skin reflectance of Asian males. Upper curve corresponds to light complexion while lower curve to dark complexion.

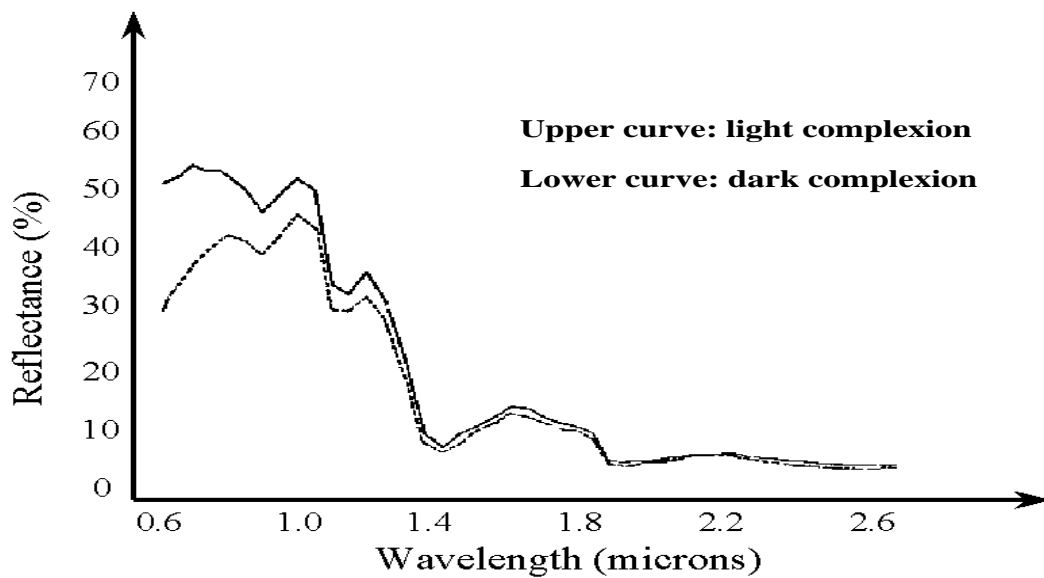


Figure 8: Skin reflectance of black males. Upper curve corresponds to light complexion while lower curve to dark complexion.

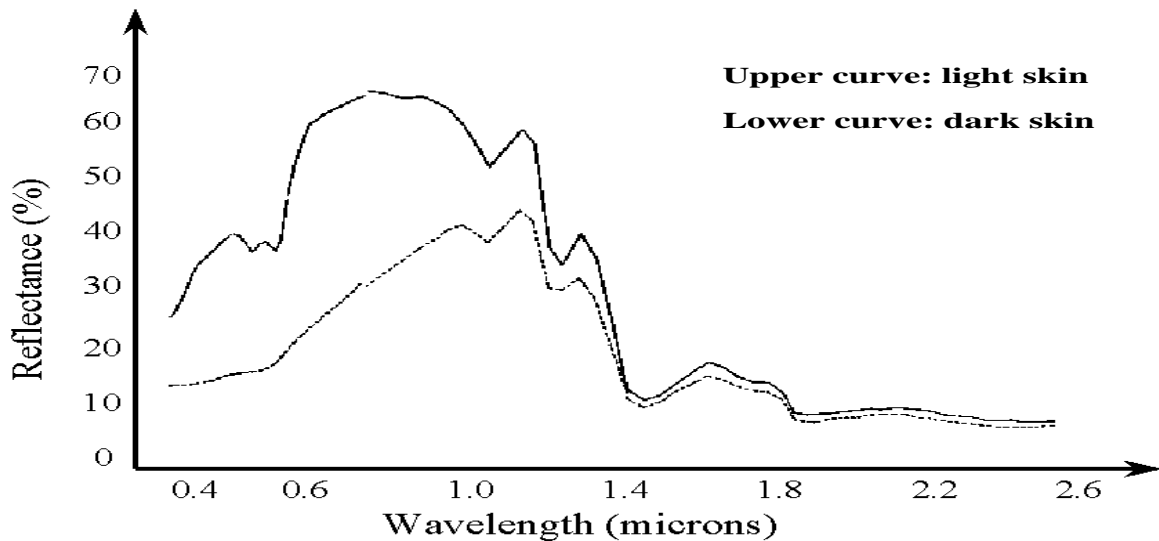


Figure 9: Reflectance of dark skin versus light skin. The lower curve corresponds to dark skin while the upper curve to light skin. Up to 1.4 μm the discrepancy between the two curves is substantial. After the 1.4 μm threshold point, however, the two curves are almost coincident. They both feature very low reflectance values in this range, which explains why everybody appears dark in the near-infrared camera operating in this band.



Figure 10: A Caucasian male and a dummy head in the range 1.4 - 1.7 μm .

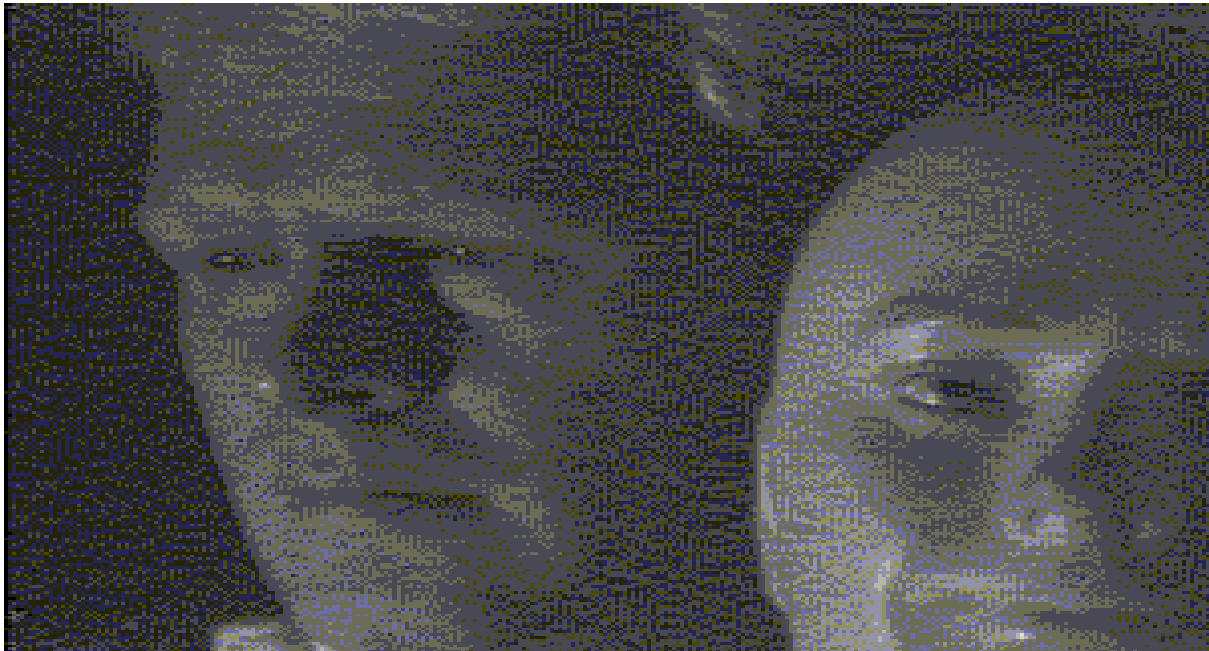


Figure 11: A Caucasian male and a dummy head in the range 1.1 - 1.4 μm .

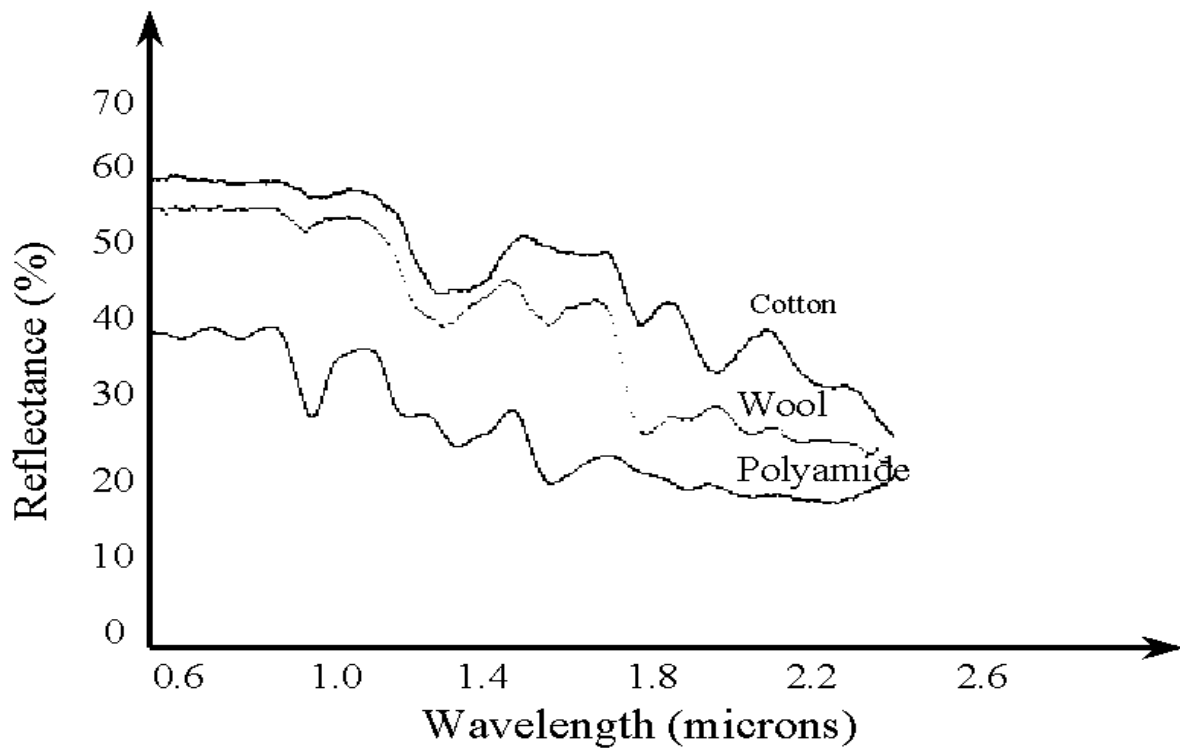


Figure 12: Reflectance of different fabric materials. The drop in reflectance after the 1.4 μm threshold point is relatively minor.

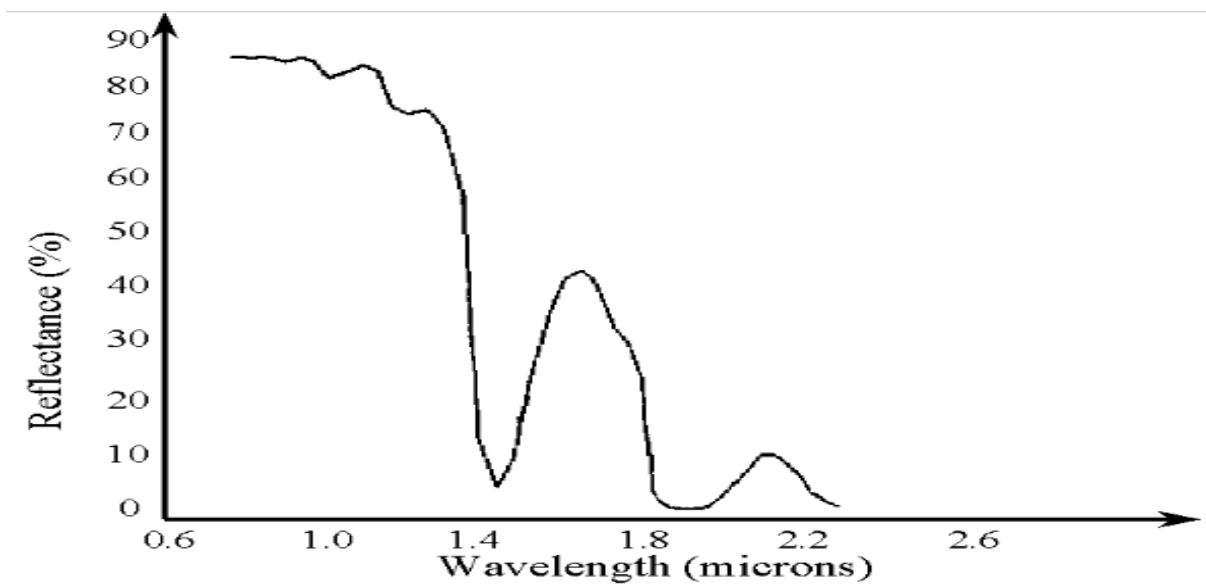


Figure 13: Reflectance of distilled water. The drop in reflectance after the 1.4 μm threshold point is substantial.

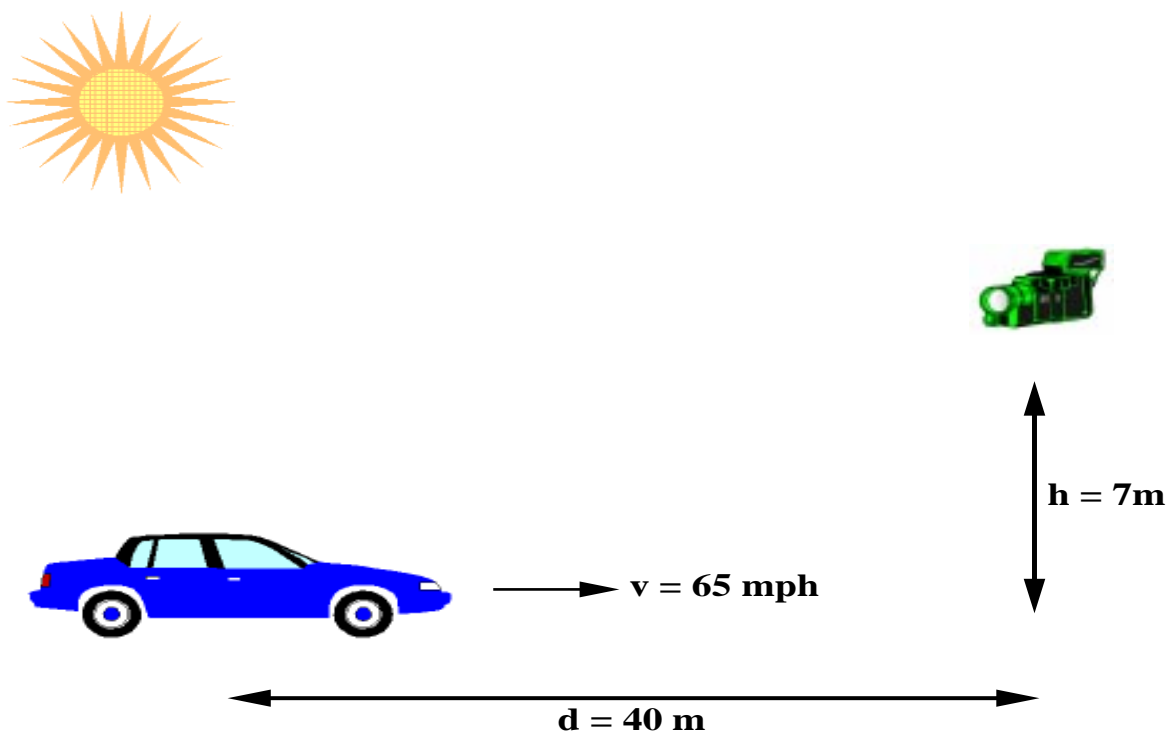


Figure 14: Sensor arrangement for daytime scenario.

List of Figures

| | |
|--|----|
| Figure 1: Electro-Magnetic (EM) spectrum..... | 12 |
| Figure 2: Transmittance of a typical windshield from 0.3 - 3.0 μm . Upper curve corresponds to a clean windshield. Lower curve corresponds to the same windshield when it gets dirty. | 12 |
| Figure 3: Transmittance of a lightly tinted side window from 0.3 - 3.0 μm . It is evident the graceful drop in transmittance even after the critical threshold of 2.8 μm . This spectral behavior allows for penetration of some thermal radiation. Compare this with the windshield transmittance in Figure 2..... | 13 |
| Figure 4: Side snapshot of a low speed car with a mid-infrared camera..... | 13 |
| Figure 5: Side snapshot of a fast moving car (65 mph) with a mid-infrared camera. The image appears heavily blurred since the speed of the camera cannot keep up with the speed of the target. | 14 |
| Figure 6: Skin reflectance of Caucasian males. Upper curve corresponds to light complexion while lower curve to dark complexion..... | 14 |
| Figure 7: Skin reflectance of Asian males. Upper curve corresponds to light complexion while lower curve to dark complexion..... | 15 |
| Figure 8: Skin reflectance of black males. Upper curve corresponds to light complexion while lower curve to dark complexion..... | 15 |
| Figure 9: Reflectance of dark skin versus light skin. The lower curve corresponds to dark skin while the upper curve to light skin. Up to 1.4 μm the discrepancy between the two curves is substantial. After the 1.4 μm threshold point, however, the two curves are almost coincident. They both feature very low reflectance values in this range, which explains why everybody appears dark in the near-infrared camera operating in this band..... | 16 |
| Figure 10: A Caucasian male and a dummy head in the range 1.4 - 1.7 μm | 16 |
| Figure 11: A Caucasian male and a dummy head in the range 1.1 - 1.4 μm | 17 |
| Figure 12: Reflectance of different fabric materials. The drop in reflectance after the 1.4 μm threshold point is relatively minor. | 17 |
| Figure 13: Reflectance of distilled water. The drop in reflectance after the 1.4 μm threshold point is substantial.... | 18 |
| Figure 14: Sensor arrangement for daytime scenario. | 18 |